

Thermal Fourier Transform Infrared Technique Quickly Detects an Early Onset of Glycation-Induced Conformational Changes of Human Serum Albumin

Yu-Ting Huang^{1,2}, Hui-Fen Liao², Shun-Li Wang³ and Shan-Yang Lin^{1*}

¹Department of Biotechnology and Pharmaceutical Technology, Yuanpei University of Medical Technology, Hsin Chu, Taiwan, ROC

²Department of Biochemical Science and Technology, National Chiayi University, Chiayi, Taiwan, ROC

³Department of Applied Chemistry, National Chiayi University, Chiayi, Taiwan, ROC

*Corresponding author: Shan-Yang Lin, Department of Biotechnology and Pharmaceutical Technology, Yuanpei University of Medical Technology, No. 306, Yuanpei street, Hsin Chu 30015, Taiwan, ROC, Tel: +886-3-6102439; Fax: +886-3-6102328; E-mail: sylin@mail.ypu.edu.tw

Received date: October 27, 2016; Accepted date: November 14, 2016; Published date: November 16, 2016

Copyright: © 2016 Yu-Ting H, et al. This is an open-access article distributed under the terms of the Creative Commons Attribution License, which permits unrestricted use, distribution, and reproduction in any medium, provided the original author and source are credited.

Abstract

Numerous potential inhibitors for prevention of advanced glycation end products (AGEs) formation have been extensively investigated for their *in vitro* and *in vivo* features, but it would spend a lot of time studying. In the present study, a unique thermal Fourier Transform Infrared (FTIR) combined system as an accelerated method was attempted to simultaneously determine the thermal-dependent conformational changes of human serum albumin (HSA) in the HSA-ribose mixture and examine the onset of the structural transformation from α -helix to β -sheet structures with or without AGEs inhibitors used. The present results clearly indicate that native HSA had an onset temperature at 96°C for the irreversible thermal-induced structural transition from α -helices to β -sheets, whereas HSA-ribose mixture exhibited its onset temperature near at 78°C due to the early occurrence of glycation. However, the onset temperature of the α -helix to β -sheet transition was gradually changed from 78°C to 96°C by increasing the amount of sodium diclofenac or inositol, which was closed to that of the onset temperature of native HSA. This implies that the thermal-induced transition from α -helix to β -sheet for HSA in the HSA-ribose mixture was effectively prevented after adding sodium or inositol. The present study also suggests that this thermal FTIR technique not only rapidly accelerates the conformational changes of HSA-ribose mixture but also directly detects onset temperature of the α -helix to β -sheet transition in real time. This unique thermal FTIR combined system could be a useful tool to screen and evaluate quickly the glycation-induced conformational changes of proteins in a one-step process.

Keywords: Human serum albumin; Advanced glycation; End products; Ribose; Thermal FTIR

Introduction

Glycation (also called non-enzymatic glycosylation) is a well-known chemical modification of proteins with reducing sugars, which may occur either inside the body (endogenous glycation) or outside the body (exogenous glycation) through the covalent bonding [1-2]. The formation of these cross-linked substances is called advanced glycation end products (AGEs) [3-4]. Several studies have shown that the formation and/or accumulation of AGEs are implicated in the progression of many age-related diseases and particularly exacerbated in aging [5-9]. Fortunately, glycation can be prevented by the natural defense system in the human body, or by natural and synthetic inhibitors [2,10-13]. Theoretically, any method or inhibitor that can inhibit any step of glycation process, prevent the formation of intermediate and/or AGEs, or scavenge free radicals, may effectively prevent or delay the existing diseases and related complications [2,14-16]. Some potential inhibitors of AGEs formation have been screened and attempted to act as a preventive medicine [17-18], however, only a few studies had been investigated to determine the biophysical properties of the glycated proteins after application of inhibitors [19-21].

All reducing sugars have been reported to react irreversibly with amino acid residues of peptides or proteins in the glycation reaction

[1-6]. The glycation reaction starts with the formation of Schiff bases, and then rearranges into Amadori products. Both Schiff bases and Amadori products are reversible reaction products. The Amadori products then undergo a series of chemical modifications to produce various irreversible intermediate compounds and finally form the AGEs products [22-24]. The glycation ability of these common reducing sugars has been found to increase in the following order: D-glucose<D-mannose<D-galactose<D-xylose<D-fructose<D-arabinose<D-ribose [25-26]. D-ribose is probably the most reactive one in the glycation of proteins, leading to a more rapid production of AGEs than other sugars *in vitro* and *in vivo* [27-29]. The glycation of proteins with ribose (also called ribosylation) has recently attracted more attention because of the protein aggregation and fibrillation, and reactive oxygen species generation in the ribosylation process [26,30-31]. The AGEs have been widely studied in clinical approaches [32-34], but the basic study on the structural conformational changes of protein after glycation is still scarce. Particularly, there is a great controversy as to whether glycation or ribosylation can alter the protein conformational structure in the glycation reaction [35-38]. Thus, it is interesting for us to further examine the changes of protein secondary conformation after ribosylation with or without AGEs inhibitors by using a specific analytical technique.

Recently, a novel Fourier Transform Infrared (FTIR) microspectroscopy equipped with a micro hot stage (thermal FTIR combined system) has been extensively applied by our groups to quickly investigate the thermal-induced structural changes in the food,

polymers, pharmaceuticals, excipients, and drug-coformer cocrystal formation [39-43]. This unique thermal FTIR combined system is a simple, quick and time-saving tool, and can simultaneously establish the correlation between the thermal response and the informative IR spectra of structural changes of the sample. In the present study, human serum albumin (HSA) was selected as a model protein and ribose was chosen as a reducing sugar. This study attempts to simultaneously determine the thermal-dependent conformational changes of HSA before and after ribose addition by using this thermal FTIR combined system as an accelerated method. Moreover, sodium diclofenac or inositol reported as an AGEs inhibitor [17-18] was also incorporated to further investigate their influences on the alterations of secondary structure of HSA in HSA-ribose mixture by this unique analytical technique.

Materials and Methods

Materials

Human serum albumin (HSA), D-ribose, sodium diclofenac, and inositol were purchased from Sigma-Aldrich Co. LLC. (St. Louis, MO, USA) and used as supplied without further purification. All the reagents were of analytical grade and were also obtained from Sigma-Aldrich Co. LLC. The potassium bromide (KBr) crystals for the pellets were obtained from Jasco Parts Center (Jasco Co., Tokyo, Japan).

Preparation of different samples for thermal FTIR determination

One drop of 50 mg/mL HSA aqueous solution with or without ribose (200 mM) and inhibitors (4-16 μ L 2.5% sodium diclofenac and 4-10 μ L 5% inositol) was dropped on glass plate, respectively, and stored at 25°C and 50% RH condition for 24 hrs. After storage for 1 day, a film was formed on the glass plate.

Transmission FTIR microspectroscopic study

A trace amount of each film sample was respectively sealed into two piece of KBr pellets (without any grinding process with KBr powders) by directly compressing with an IR spectrophotometric hydraulic press (Riken Seiki Co., Tokyo, Japan) under 400 kg cm^2 for 15 s. The compressed KBr disk was determined by FTIR microspectroscopy (IRT-5000-16/FTIR-6200, Jasco Co., Tokyo, Japan) with a mercury cadmium telluride (MCT) detector by transmission technique to get the FTIR spectrum of each sample [44-45]. All FTIR spectra were generated by co-addition of 256 interferograms collected at 4 cm^{-1} resolution. Three runs were performed.

Thermal FTIR microspectroscopic study

A compressed KBr disc containing each film sample was placed directly onto a micro hot stage (DSC microscopy cell, FP 84, Mettler, Greifensee, Switzerland) and directly determined by FTIR microspectroscopy (IRT-5000-16/FTIR-6200, Jasco Co., Tokyo, Japan) with a MCT detector. The operation was performed in the transmission mode [39,44-45]. FTIR spectra were generated by co-addition of 256 interferograms collected at 4 cm^{-1} resolution. The temperature of the DSC microscopy cell was monitored with a central processor (FP 80HT, Mettler, Switzerland). The heating rate of the DSC assembly was maintained at 3°C/min under ambient conditions. The compressed KBr disc was previously equilibrated to the starting

temperature (30°C) and then heated from 30 to 200°C. At the same time, the thermal-responsive IR spectra were recorded when the sample disc was heated on the DSC micro hot stage. The heated sample disc was then cooled to 25°C for further use. Each film sample was determined in triplicate.

FTIR data acquisition and handling

The software, Spectral Manager for Windows (Jasco Co., Tokyo, Japan) and GRAMS spectroscopy software suite (Version 7, Thermo Electron Co., MA, USA), were used for data acquisition and handling. Second derivative spectral analysis was applied to locate the position of the overlapping components in the amide bands and assigned to different secondary structures. The protein secondary structure and the composition of each component in the amide I band of the IR spectra were also quantitatively estimated by a least-squares fitting program iterating the curve-fitting process using a Gaussian function. The curve fitting was performed by stepwise iterative adjustment towards minimum standard errors of the different parameters determining the shape and position of the absorption peaks. Finally, the proportion of a component was computed to be the fractional area of the corresponding peak divided by the sum of the areas of all the peaks [46-48]. All the tests were conducted in triplicate and the mean values with standard deviations were obtained.

Statistical analysis

Statistical difference between the experimental groups was determined with the Student's T-test and a p-value below 0.05 was considered significant.

Results and Discussion

Human serum albumin (HSA) has been always used as a model for protein-folding and ligand-binding studies because it is the most abundant protein in human blood plasma or serum [49-50]. Glycation has been reported to alter the structure of HSA, leading to significant changes in biochemical, biophysical, and thermodynamic properties and drug-protein binding of HSA [50-55]. In our previous studies, the effects of ethanol and/or captopril on the secondary structure of HSA before and after protein binding had been investigated by FTIR determination [46-47]. Moreover, a marked change in the secondary conformational structure and protein aggregation of HSA after ribosylation had also been found [48]. In the present study, the thermal dependent-conformational changes of HSA after ribosylation with or without pretreatment of an AGEs inhibitor were attempted using a thermal FTIR combined system.

The representative FTIR spectra of native HSA, ribose, and HSA-ribose mixture were obtained over the frequency range between 1800 and 800 cm^{-1} , as shown in Figure 1. The characteristic IR absorption bands and their assignments for native HAS.

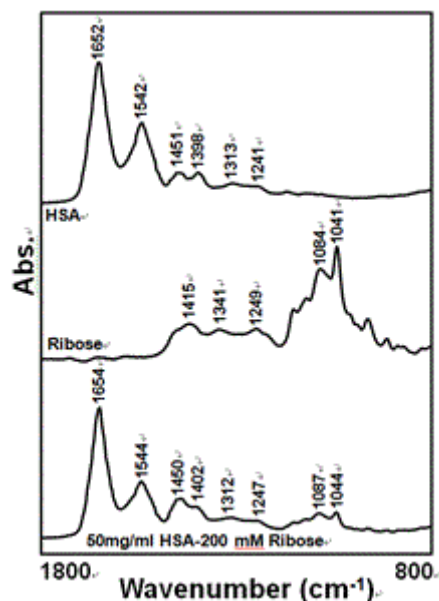


Figure 1: Representative FTIR spectra of native HSA, ribose, and HSA-ribose mixture (50 mg/mL-200 mM) determined by a film method compressed within two KBr discs via a transmission FTIR technique follows: 1652 cm^{-1} (amide I, C=O stretching), 1542 cm^{-1} (amide II, C-N stretching and N-H bending), 1451 cm^{-1} (C-H₂ bending), 1398 cm^{-1} (carboxylate) and 1313-1241 cm^{-1} (Amide III, C-N stretching and N-H bending) [56].

The spectral range within 1500-800 cm^{-1} is the fingerprint region of native HSA. While the FTIR spectrum of ribose shows strong peaks between 1200 and 1000 cm^{-1} . Both peaks at 1084 cm^{-1} assigned to C-O and C-C stretching vibrations and 1041 cm^{-1} attributed to C-OH and C-C-O bending vibrations for ribose can be used to distinguish ribose from HSA [48,57]. Once ribose was mixed with HSA, the FTIR spectrum of the HSA-ribose mixture was almost superimposed by the FTIR spectra of HSA and ribose. Two marked FTIR peaks at 1087 and 1044 cm^{-1} were attributed to ribose, other FTIR peaks were belonged to HSA.

Thermal-dependent FTIR spectral changes of native HSA with or without ribose

Thermal-dependent FTIR spectral changes of native HSA and HSA-ribose mixture in the heating processes were plotted three-dimensionally in Figure 2. It clearly indicates that the peak intensity of the amide I peak at 1652 cm^{-1} assigned to the α -helix conformation of native HSA was almost maintained at a constant level in the initial heating process, but this peak at about 96°C was split into two peaks, 1656 and 1628 cm^{-1} (Figure 2A). The former was due to the α -helix conformation at higher temperature, the latter was attributed to the β -sheet structure [58-60].

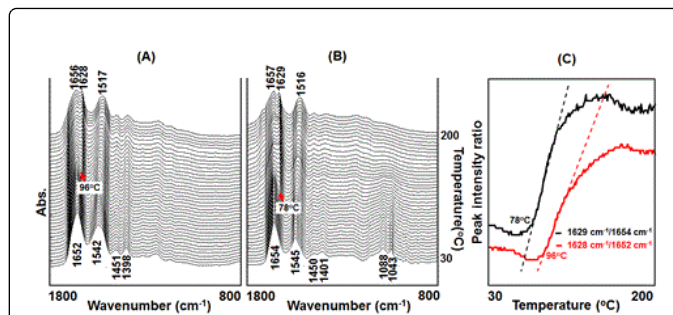


Figure 2: Thermal-dependent FTIR spectral changes of native HSA (A) and HSA-ribose mixture (B) as a function of temperature.

This suggests that a conformational transition from a α -helix to the β -sheet structure was occurred at 96°C. While the amide I peak at 1542 cm^{-1} was gradually shifted to 1517 cm^{-1} in the heating process, due to the dissociation of hydrogen bonding by thermal effect. On the other hand, similar thermal behaviour was also found for the HSA-ribose mixture but the split temperature was changed to 78°C (Figure 2B). This indicates that the thermally induced α -helix to β -sheet transition in HSA-ribose mixture was prior to that of the native HSA, implying that ribosylation might easily accelerate the conformational change of HSA in the HSA-ribose mixture during heating. The thermal-dependent peak intensity ratio of 1628 cm^{-1} /1652 cm^{-1} for native HSA was more clearly displayed an onset temperature at 96°C, while the ratio of 1629 cm^{-1} /1654 cm^{-1} for HSA-ribose mixture was shown at 78°C (Figure 2C). The secondary conformational change of HSA-ribose mixture was clearly observed much earlier than that of native HSA sample, suggesting that ribose might accelerate the time of onset of HSA glycation in the heating process by determination with thermal FTIR combined system, The results also highlight the potential use of a simultaneous thermal FTIR combined system to screen and detect the onset transition temperature of glycation-induced conformational changes of HSA in a one-step process.

The curve-fitted amide I band of native HSA or HSA-ribose mixture before and after heating processes

The IR amide I band of proteins is well known to be more sensitive than the other amide bands in the protein secondary structural components [56,58,61]. Figure 3 shows the curve-fitted amide I band of native HSA before and after heat treatment. The curve-fitted amide I bands of native HSA and their components, assignments, and compositions are also shown. The structural composition of native HSA before heat treatment consists of 44.13 \pm 3.38% α -helix (1656 cm^{-1}), 5.92 \pm 0.78% random coil (1645 cm^{-1}), 22.19 \pm 0.70% β -turn (1683 and 1673 cm^{-1}) and 27.76 \pm 1.14% β -sheet (1692, 1637, 1625 and 1612 cm^{-1}), in which 1625 and 1612 cm^{-1} were corresponded to the intermolecular β -sheet of protein aggregation and side chain [62-63]. Once the native HSA was preheated to 200°C and then cooled, on the other hand, the heated HSA yielded the following compositions of secondary structures: 25.26 \pm 2.89% α -helix, 11.32 \pm 1.56% random coil, 23.27 \pm 1.03% β -turn and 40.15 \pm 1.14% β -sheet, respectively. Obviously, the α -helical structure was markedly reduced from 44.13 \pm 3.38% to 25.26 \pm 2.89% ($p < 0.05$), whereas β -sheet structure was increased from 27.76 \pm 1.14% to 40.15 \pm 1.14% ($p < 0.05$). In addition, the random coil structure was also increased from 5.92 \pm 0.78% to 11.32 \pm 1.56% ($p < 0.05$). This implies that a α -helix to β -sheet

conversion in native HSA might be easily occurred in the heating process. Moreover, this conformational change in native HSA was the kinetically irreversible conversion.

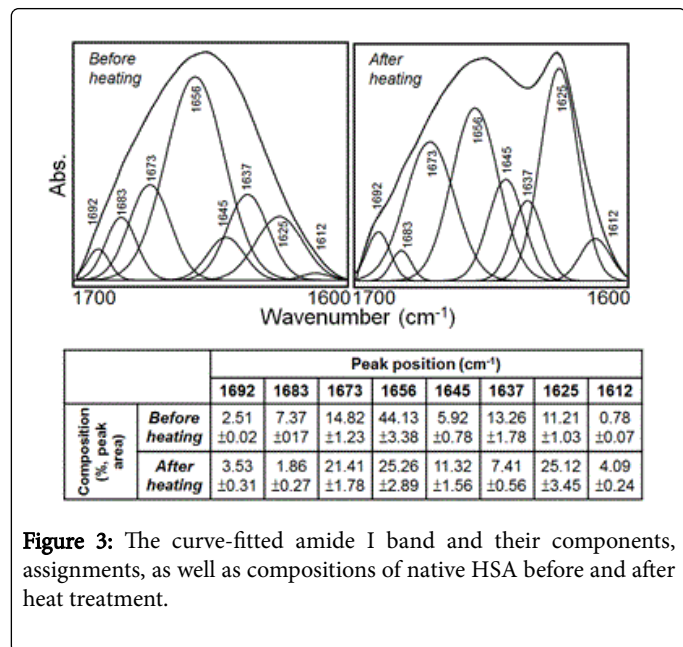


Figure 3: The curve-fitted amide I band and their components, assignments, as well as compositions of native HSA before and after heat treatment.

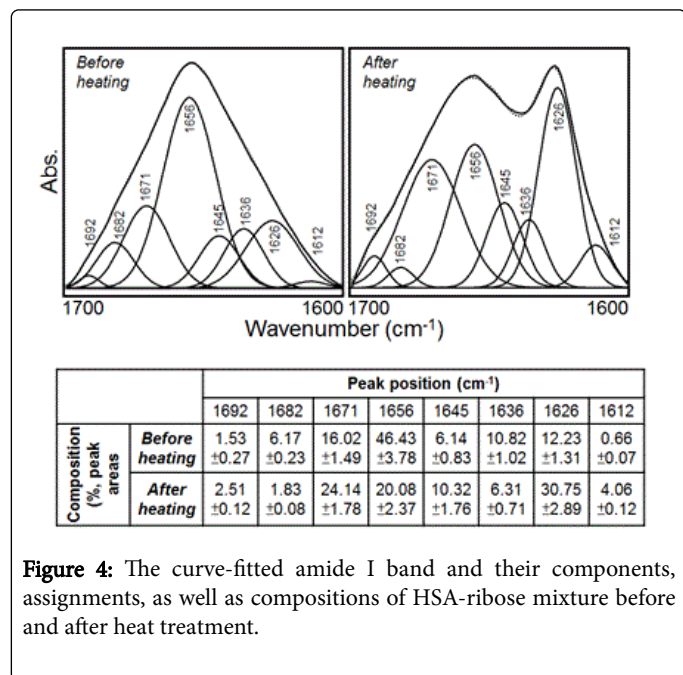


Figure 4: The curve-fitted amide I band and their components, assignments, as well as compositions of HSA-ribose mixture before and after heat treatment.

Figure 4 shows the curve-fitted amide I band of HSA-ribose mixture before and after heat treatment. The structural compositions of HSA-ribose mixture before heating exhibited similar contents to that of native HSA before heating ($p > 0.05$), suggesting that there were no alterations in HSA conformation at the initial stage of ribose added. However, the structural composition of HSA-ribose mixture after heat treatment was markedly altered. It is evident that the α -helix composition of the heated HSA-ribose mixture after cooling to room temperature was decreased from $46.43 \pm 3.78\%$ to $20.08 \pm 2.37\%$ ($p < 0.05$), but the content of β -sheet content was increased from $25.24 \pm 0.62\%$ to $43.63 \pm 0.86\%$ ($p < 0.05$). In addition, the random coil

structure was also increased from $6.14 \pm 0.83\%$ to $10.32 \pm 1.76\%$ ($p < 0.05$), but the β -turn content was slightly changed from $22.19 \pm 0.86\%$ to $25.97 \pm 0.91\%$ ($p < 0.05$). The results also clearly demonstrate that HSA-ribose mixture after heat treatment might cause more loss of helical content and increase the amount of β -sheet and β -turn structures. The ribosylation is responsible for the conformational changes, leading to an increase in total β -conformation, particularly the excess increases in the formation of intermolecular beta-sheet structures. This was consistent with the results of glycated albumin due to the conformational change from its native α -helical to β -sheeted structures [64-65], resulting in the formation of protein aggregation and fibrillation [65-68].

Effects of AGEs inhibitors on thermal-dependent conformational changes of HSA-ribose mixture

A number of natural or synthetic compounds have been proposed to act as AGEs inhibitors or breakers for therapeutic treatment of AGEs-related diseases [10-21,69]. From the results of Figure 2, a novel acceleration system was applied to exactly determine the onset transition temperature at 78°C for HSA-ribose mixture via structural transformation from α -helix to β -sheet structures, as compared to that of the onset transition temperature at 96°C for native HSA. In order to investigate whether sodium diclofenac or inositol (as an AGEs inhibitor) can modify the onset transition temperature and protein conformational structure of HSA in the HSA-ribose mixture, the thermal FTIR combined system was also attempted. Because there were less absorption peaks in the wavenumber ranges of $1800\text{-}1600\text{ cm}^{-1}$ for sodium diclofenac and inositol (data not shown), thus the amide I spectral region (range from $1750\text{ to }1595\text{ cm}^{-1}$) of HSA-ribose mixture was chosen to study their onset transition temperature and thermal-dependent conformational changes of HSA-ribose mixture with different amounts of sodium diclofenac or inositol.

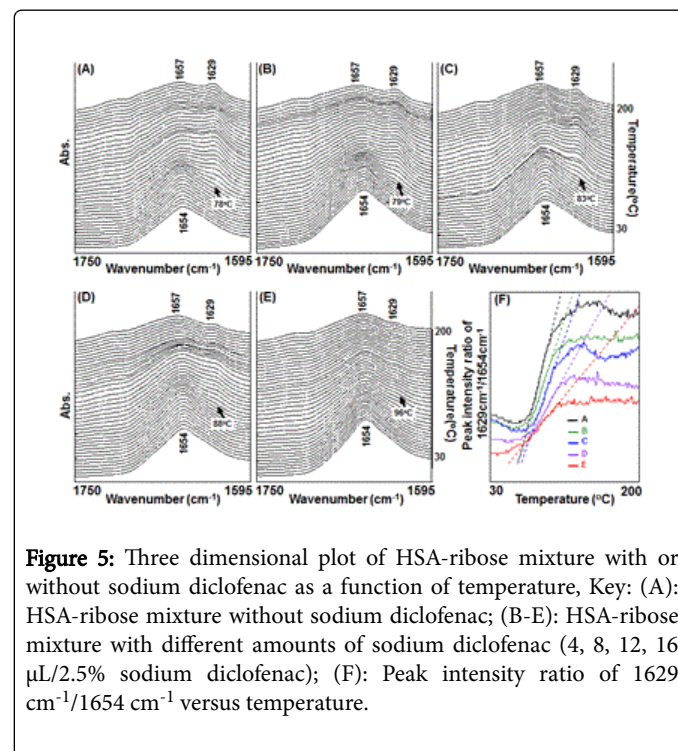


Figure 5: Three dimensional plot of HSA-ribose mixture with or without sodium diclofenac as a function of temperature, Key: (A): HSA-ribose mixture without sodium diclofenac; (B-E): HSA-ribose mixture with different amounts of sodium diclofenac (4, 8, 12, 16 $\mu\text{L}/2.5\%$ sodium diclofenac); (F): Peak intensity ratio of $1629\text{ cm}^{-1}/1654\text{ cm}^{-1}$ versus temperature.

Figure 5 shows the three dimensional plot of HSA-ribose mixture with or without sodium diclofenac as a function of temperature, in which the onset temperature at 78°C for α -helix to β -sheet transition was observed for the HSA-ribose mixture without sodium diclofenac (Figure 5A). However, it demonstrates that the onset transition temperature was gradually changed from 78°C to 96°C by increasing the amount of sodium diclofenac used (Figures 5B-5E). This was closed to that of the onset temperature at 96°C of native HSA. From the slope data for the peak intensity ratio profile of different samples, the gradual slope decline was clearly observed with the increase of sodium diclofenac added (Figures 5F and 6A). This implies that thermal-induced secondary conformational change of HSA in HSA-ribose mixture was effectively prevented by adding the AGEs inhibitor of sodium diclofenac via thermal FTIR determination.

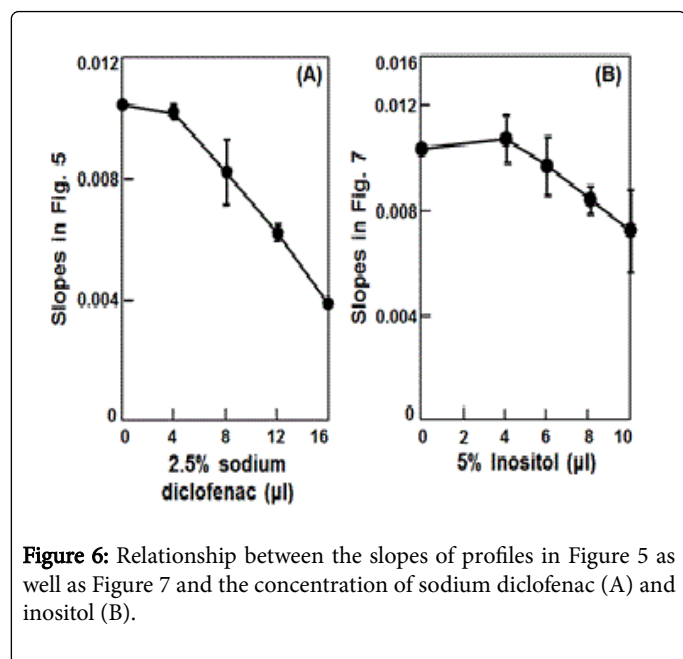


Figure 6: Relationship between the slopes of profiles in Figure 5 as well as Figure 7 and the concentration of sodium diclofenac (A) and inositol (B).

Figures 6 and 7 also exhibited that inositol might prevent the thermal-induced conformation changes from α -helix to β -sheet transition of HSA in HSA-ribose mixture. As compared in Figure 6, sodium diclofenac seems to be more effective than that of inositol for preventing these thermal-induced conformation changes.

Our data are consistent with the inhibitory effect of sodium diclofenac or inositol reported [18,70-72]. Diclofenac has been proposed to inhibit the sugar attachment on HSA by specifically blocking at least one of the major glycation sites of HSA [18,70]. The higher the concentration of sodium diclofenac used the more the blocking glycation sites obtained, leading to a decrease in slope gradient but an increase in onset transition temperature for HSA-ribose mixture in the present study. On the other hand, inositol has also been proposed as an antioxidant and/or antiglycating agent to delay and/or avert the glycation of HSA-ribose mixture [18,71-72], which can probably be verified by present study.

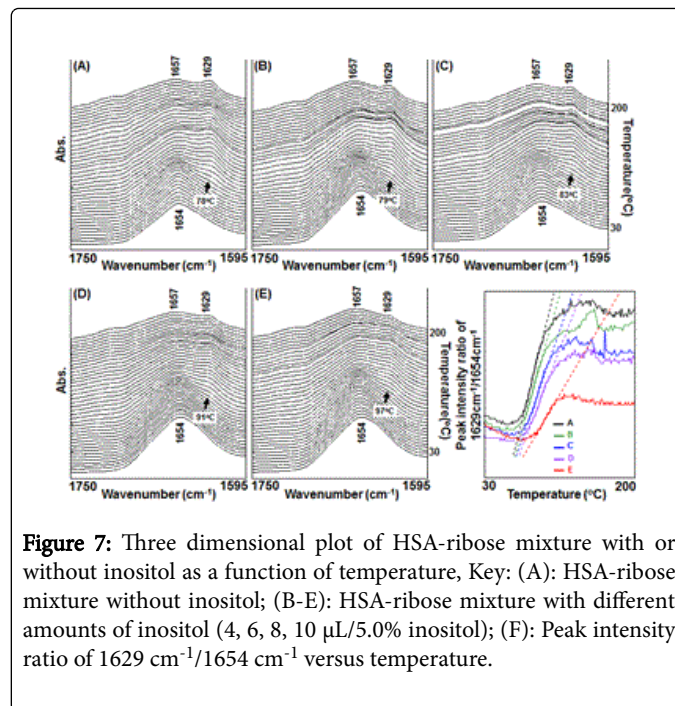


Figure 7: Three dimensional plot of HSA-ribose mixture with or without inositol as a function of temperature, Key: (A): HSA-ribose mixture without inositol; (B-E): HSA-ribose mixture with different amounts of inositol (4, 6, 8, 10 µL/5.0% inositol); (F): Peak intensity ratio of 1629 cm⁻¹/1654 cm⁻¹ versus temperature.

Conclusion

Thermal FTIR technique was first attempted to investigate the thermal-induced conformational changes of HSA in HSA-ribose mixture before and after addition of AGEs inhibitor, sodium diclofenac or inositol. Native HSA had the onset temperature located at 96°C for the irreversible structural transition of α -helix to β -sheet. While HSA-ribose exhibited its onset temperature near at 78°C, due to the thermal acceleration. By incorporating sodium diclofenac or inositol, however, the onset transition temperature was gradually changed from 78°C to 96°C with the increase of sodium diclofenac or inositol added, near to that of the onset temperature of native HSA. This implies that thermal-induced α -helix to β -sheet transition in the secondary conformational structure of HSA in HSA-ribose mixture was effectively prevented by adding sodium diclofenac or inositol. This unique thermal FTIR combined system could be a sensitive and potentially useful tool for rapid evaluation of the glycation-induced conformational changes of proteins with or without AGEs inhibitors. The relationship between thermal-dependent conformational changes of HSA and *in vitro/in vivo* inhibitory effect of AGEs inhibitors would need to be further studied.

Declaration of Conflicting Interests

The authors declared no potential conflicts of interest with respect to the research, authorship, and/or publication of this article.

Funding

The authors received no financial support for the research, authorship, and/or publication of this article.

References

1. Rabbani N, Thornalley PJ (2012) Glycation research in amino acids: a place to call home. *Amino Acids* 42: 1087-1096.

2. Younus H, Anwar S (2016) Prevention of non-enzymatic glycosylation (glycation): Implication in the treatment of diabetic complication. *Int J Health Sci (Qassim)* 10: 261-277.
3. Singh R, Barden A, Mori T, Beilin L (2001) Advanced glycation end-products: a review. *Diabetologia* 44: 129-146.
4. Sharma C, Kaur A, Thind SS, Singh B, Raina S (2015) Advanced glycation End-products (AGEs): an emerging concern for processed food industries. *J Food Sci Technol* 52: 7561-7576.
5. Simm A, Müller B, Nass N, Hofmann B, Bushnaq H, et al. (2015) Protein glycation - Between tissue aging and protection. *Exp Gerontol* 68: 71-75.
6. Ramasamy R, Vannucci SJ, Yan SS, Herold K, Yan SF, et al. (2005) Advanced glycation end products and RAGE: a common thread in aging, diabetes, neurodegeneration, and inflammation. *Glycobiology* 15: 16R-28R.
7. Ajith TA, Vinodkumar P (2016) Advanced glycation end products: Association with the pathogenesis of diseases and the current therapeutic advances. *Curr Clin Pharmacol* 11: 118-127.
8. Arasteh A, Farahi S, Habibi-Rezaei M, Moosavi-Movahedi AA (2014) Glycated albumin: an overview of the *in vitro* models of an *in vivo* potential disease marker. *J Diabetes Metab Disord* 13: 49.
9. Uribarri J, del Castillo MD, de la Maza MP, Filip R, Gugliucci A, et al. (2015) Dietary advanced glycation end products and their role in health and disease. *Adv Nutr* 6: 461-473.
10. Peng X, Ma J, Chen F, Wang M (2011) Naturally occurring inhibitors against the formation of advanced glycation end-products. *Food Funct* 2: 289-301.
11. Elost A, Ghous T, Ahmed N (2012) Natural products as anti-glycation agents: possible therapeutic potential for diabetic complications. *Curr Diabetes Rev* 8: 92-108.
12. Abbas G, Al-Harrasi AS, Hussain H, Hussain J, et al. (2016) Antiglycation therapy: Discovery of promising antiglycation agents for the management of diabetic complications. *Pharm Biol* 54: 198-206.
13. Jahan H, Choudhary MI (2015) Glycation, carbonyl stress and AGEs inhibitors: a patent review. *Expert Opin Ther Pat* 25: 1267-1284.
14. Salahuddin P, Rabbani G, Khan RH (2014) The role of advanced glycation end products in various types of neurodegenerative disease: a therapeutic approach. *Cell Mol Biol Lett* 19: 407-437.
15. Aldini G, Vistoli G, Stefek M, Chondrogianni N, Grune T, et al. (2013) Molecular strategies to prevent, inhibit, and degrade advanced glycoxidation and advanced lipoxidation end products. *Free Radic Res* 47: 93-137.
16. Wu CH, Huang SM, Lin JA, Yen GC (2011) Inhibition of advanced glycation endproduct formation by foodstuffs. *Food Funct* 2: 224-234.
17. Alam S, Ahsan A, Alam S (2013) Newer insights in drugs inhibiting formation and accumulation of advanced glycation end products. *J Biochem Tech* 5: 666-672.
18. Rahbar S, Figarola JL (2003) Novel inhibitors of advanced glycation endproducts. *Arch Biochem Biophys* 419: 63-79.
19. Annibal A, Riemer T, Jovanovic O, Westphal D, Griesser E, et al. (2016) Structural, biological and biophysical properties of glycated and glycoxidized phosphatidylethanolamines. *Free Radic Biol Med* 95: 293-307.
20. Ma H, Liu W, Frost L, Wang L, Kong L, et al. (2015) The hydrolyzable gallotannin, penta-O-galloyl-β-D-glucopyranoside, inhibits the formation of advanced glycation endproducts by protecting protein structure. *Mol Biosyst* 11: 1338-1347.
21. Iannuzzi C, Irace G, Sirangelo I (2014) Differential effects of glycation on protein aggregation and amyloid formation. *Front Mol Biosci* 1: 9.
22. Horvat S, Jakas A (2004) Peptide and amino acid glycation: new insights into the Maillard reaction. *J Pept Sci* 10: 119-137.
23. Takahashi M (2014) Glycation of Proteins. In *Glycoscience: Biology and Medicine* pp: 1339-1345.
24. Nursten HE (2005) The Maillard Reaction: Chemistry, Biochemistry, and Implications. *RSC* 58: 756.
25. Monnier VM (1990) Nonenzymatic glycosylation, the Maillard reaction and the aging process. *J Gerontol* 45: B105-B111.
26. Wei Y, Han CS, Zhou J, Liu Y, Chen L, et al. (2012) D-ribose in glycation and protein aggregation. *Biochim Biophys Acta* 1820: 488-494.
27. Monnier VM, Cerami A (1981) Nonenzymatic browning *in vivo*: possible process for aging of long-lived proteins. *Science* 211: 491-493.
28. Han C, Lu Y, Wei Y, Liu Y, He R (2011) D-ribose induces cellular protein glycation and impairs mouse spatial cognition. *PLoS One* 6: e24623.
29. Syrový I (1994) Glycation of albumin: reaction with glucose, fructose, galactose, ribose or glyceraldehyde measured using four methods. *J Biochem Biophys Methods* 28: 115-121.
30. Kong FL, Cheng W, Chen J, Liang Y (2011) d-Ribose glycates I²(2)-microglobulin to form aggregates with high cytotoxicity through a ROS-mediated pathway. *Chem Biol Interact* 194: 69-78.
31. Khan MS, Dwivedi S, Priyadarshini M, Tabrez S, Siddiqui MA, et al. (2013) Ribosylation of bovine serum albumin induces ROS accumulation and cell death in cancer line (MCF-7). *Eur Biophys J* 42: 811-818.
32. Nenna A, Nappi F, Avtaar Singh SS, Sutherland FW, Di Domenico F, et al. (2015) Pharmacologic Approaches Against Advanced Glycation End Products (AGEs) in Diabetic Cardiovascular Disease. *Res Cardiovasc Med* 4: e26949.
33. Greven WL, Smit JM, Rommes JH, Spronk PE (2010) Accumulation of advanced glycation end (AGEs) products in intensive care patients: an observational, prospective study. *BMC Clin Pathol* 10: 4.
34. Goh SY1, Cooper ME (2008) Clinical review: The role of advanced glycation end products in progression and complications of diabetes. *J Clin Endocrinol Metab* 93: 1143-1152.
35. Iannuzzi C, Maritato R, Irace G, Sirangelo I (2013) Glycation accelerates fibrillization of the amyloidogenic W7FW14F apomyoglobin. *PLoS One* 8: e80768.
36. Adrover M, Mariño L, Sanchis P, Pauwels K, Kraan Y, et al. (2014) Mechanistic insights in glycation-induced protein aggregation. *Biomacromolecules* 15: 3449-3462.
37. Liu J, Ru Q, Ding Y (2012) Glycation a promising method for food protein modification: Physicochemical properties and structure, a review. *Food Res Int* 49: 170-183.
38. Wei Y, Chen L, Chen J, Ge L, He RQ (2009) Rapid glycation with D-ribose induces globular amyloid-like aggregations of BSA with high cytotoxicity to SH-SY5Y cells. *BMC Cell Biol* 10: 10.
39. Lin SY, Wang SL (2012) Advances in simultaneous DSC-FTIR microspectroscopy for rapid solid-state chemical stability studies: some dipeptide drugs as examples. *Adv Drug Deliv Rev* 64: 461-478.
40. Lin SY (2015) Molecular perspectives on solid-state phase transformation and chemical reactivity of drugs: metoclopramide as an example. *Drug Discov Today* 20: 209-222.
41. Lin SY, Lin CC (2016) One-step Real-time Food Quality Analysis by Simultaneous DSC-FTIR Microspectroscopy. *Crit Rev Food Sci Nutr* 56: 292-305.
42. Lin SY (2016) An overview of advanced hyphenated techniques for simultaneous analysis and characterization of polymeric materials. *Crit Rev Solid State Mater Sci* 41: 482-530.
43. Lin SY (2016) Mechanochemical Approaches to Pharmaceutical Cocrystal Formation and Stability Analysis. *Curr Pharm Des* 22: 5001-5018.
44. Lin HL, Huang YT, Lin SY (2016) Spectroscopic and thermoanalytical evidence of a formation mechanism of piroxicam-saccharin co-crystal Induced by solvent-assisted grinding or thermal stress. *J Therm Anal Calorim* 123: 2345-2356.
45. Huang DF, Hsieh TF, Lin SY (2013) One-step simultaneous DSC-FTIR microspectroscopy to quickly detect continuous pathways in solid-state glucose/asparagine Maillard reaction. *J AOAC Int* 96: 1362-1364.
46. Lin SY, Wei YS, Li MJ, Wang SL (2004) Effect of ethanol or/and captopril on the secondary structure of human serum albumin before and after protein binding. *Eur J Pharm Biopharm* 57: 457-464.

47. Lin SY, Wei YS, Li MJ (2004) Ethanol or/and captopril-induced precipitation and secondary conformational changes of human serum albumin. *Spectrochim Acta A* 60: 3107-3111.
48. Huang YT, Liao HF, Wang SL, Lin SY (2016) Glycation and secondary conformational changes of human serum albumin: study of the FTIR spectroscopic curve-fitting technique. *AIMS Biophys* 3: 247-260.
49. Kragh-Hansen U, Chuang VT, Otagiri M (2002) Practical aspects of the ligand-binding and enzymatic properties of human serum albumin. *Biol Pharm Bull* 25: 695-704.
50. Mendez DL, Jensen RA, McElroy LA, Pena JM, Esquerra RM (2005) The effect of non-enzymatic glycation on the unfolding of human serum albumin. *Arch Biochem Biophys* 444: 92-99.
51. Anguizola J, Matsuda R, Barnaby OS, Hoy KS, Wa C, et al. (2013) Review: Glycation of human serum albumin. *Clin Chim Acta* 425: 64-76.
52. Ueda Y, Matsumoto H (2015) Recent topics in chemical and clinical research on glycated albumin. *J Diabetes Sci Technol* 9: 177-182.
53. Szkudlarek A, Sulkowska A, Maciazek-Jurczyk M, Chudzik M, Równicka-Zubik J (2016) Effects of non-enzymatic glycation in human serum albumin. Spectroscopic analysis. *Spectrochim Acta A Mol Biomol Spectrosc* 152: 645-653.
54. Khan MW, Rasheed Z, Khan WA, Ali R (2007) Biochemical, biophysical, and thermodynamic analysis of *in vitro* glycated human serum albumin. *Biochemistry (Mosc)* 72: 146-152.
55. Cao H, Chen T, Shi Y (2015) Glycation of human serum albumin in diabetes: impacts on the structure and function. *Curr Med Chem* 22: 4-13.
56. Yang H, Yang S, Kong J, Dong A, Yu S (2015) Obtaining information about protein secondary structures in aqueous solution using Fourier transform IR spectroscopy. *Nat Protoc* 10: 382-396.
57. Lu Y, Deng G, Miao F, Li Z (2003) Metal ion interactions with sugars. The crystal structure and FT-IR study of the NdCl₃-ribose complex. *Carbohydr Res* 338: 2913-2919.
58. Haris PI (2013) Probing protein-protein interaction in biomembranes using Fourier transform infrared spectroscopy. *Biochim Biophys Acta* 1828: 2265-2271.
59. Neault JF, Tajmir-Riahi HA (1998) Interaction of cisplatin with human serum albumin. Drug binding mode and protein secondary structure. *Biochim Biophys Acta* 1384: 153-159.
60. Bramanti E, Benedetti E (1996) Determination of the secondary structure of isomeric forms of human serum albumin by a particular frequency deconvolution procedure applied to Fourier transform IR analysis. *Biopolymers* 38: 639-653.
61. Kong J, Yu S (2007) Fourier transform infrared spectroscopic analysis of protein secondary structures. *Acta Biochim Biophys Sin* 39: 549-559.
62. Imamura K, Ohyama K, Yokoyama T, Maruyama Y, Kazuhiro N (2009) Temperature scanning FTIR analysis of secondary structures of proteins embedded in amorphous sugar matrix. *J Pharm Sci* 98: 3088-3098.
63. Litvinov RI, Faizullin DA, Zuev YF, Weisel JW (2012) The α -helix to β -sheet transition in stretched and compressed hydrated fibrin clots. *Biophys J* 103: 1020-1027.
64. GhoshMoulick R, Bhattacharya J, Roy S, Basak S, Dasgupta AK (2007) Compensatory secondary structure alterations in protein glycation. *Biochim Biophys Acta* 1774: 233-242.
65. Bouma B, Kroon-Batenburg LM, Wu YP, Brünjes B, Posthuma G, et al. (2003) Glycation induces formation of amyloid cross-beta structure in albumin. *J Biol Chem* 278: 41810-41819.
66. Khan TA, Saleemuddin M, Naeem A (2011) Partially folded glycated state of human serum albumin tends to aggregate. *Int J Pept Res Ther* 17: 271-279.
67. Jindal S, Naeem A (2013) Consequential secondary structure alterations and aggregation during prolonged casein glycation. *J Fluoresc* 23: 367-374.
68. Lin SY, Chu HL, Wei YS (2002) Pressure-induced transformation of alpha-helix to beta-sheet in the secondary structures of amyloid beta (1-40) peptide exacerbated by temperature. *J Biomol Struct Dyn* 19: 619-625.
69. Nagai R, Murray DB, Metz TO, Baynes JW (2012) Chelation: a fundamental mechanism of action of AGE inhibitors, AGE breakers, and other inhibitors of diabetes complications. *Diabetes* 61: 549-559.
70. van Boekel MA, van den Bergh PJ, Hoenders HJ (1992) Glycation of human serum albumin: inhibition by Diclofenac. *Biochim Biophys Acta* 1120: 201-204.
71. Ramakrishnan S, Sulochana KN, Punitham R (1999) Two new functions of inositol in the eye lens: antioxidation and antiglycation and possible mechanisms. *Indian J Biochem Biophys* 36: 129-133.
72. Sulochana KN, Ramprasad S, Coral K, Lakshmi S, Punitham R, et al. (2003) Glycation and glycooxidation studies *in vitro* on isolated human vitreous collagen. *Med Sci Monit* 9: BR220-BR224.